

Giant Outer Transiting Exoplanet Mass (GOT ‘EM) Survey. V. Two Giant Planets in Kepler-511 but Only One Ran Away

YAYAATI CHACHAN ^{1,2,*}, PAUL A. DALBA ³, DANIEL P. THORNGREN ⁴, STEPHEN R. KANE ⁵, EVE J. LEE ^{1,2},
EDWARD W. SCHWIETERMAN ⁵, HOWARD ISAACSON ^{6,7}, ANDREW W. HOWARD ⁸, AND MATTHEW J. PAYNE ⁹

¹*Department of Physics and Trottier Space Institute, McGill University, 3600 rue University, H3A 2T8 Montréal, QC, Canada*

²*Trottier Institute for Research on Exoplanets (iREx), Université de Montréal, Quebec, Canada*

³*Department of Astronomy and Astrophysics, University of California, Santa Cruz, CA 95064, USA*

⁴*Department of Physics & Astronomy, Johns Hopkins University, Baltimore, MD 21210, USA*

⁵*Department of Earth and Planetary Sciences, University of California Riverside, 900 University Ave, Riverside, CA 92521, USA*

⁶*Department of Astronomy, University of California Berkeley, Berkeley CA 94720, USA*

⁷*Centre for Astrophysics, University of Southern Queensland, Toowoomba, QLD, Australia*

⁸*Department of Astronomy, California Institute of Technology, Pasadena, CA 91125, USA*

⁹*Harvard-Smithsonian Center for Astrophysics, 60 Garden St., MS 51, Cambridge, MA 02138, USA*

ABSTRACT

Systems hosting multiple giant planets are important laboratories for understanding planetary formation and migration processes. We present a nearly decade-long Doppler spectroscopy campaign from the Keck-I telescope to characterize the two transiting giant planets orbiting Kepler-511 on orbits of 27 days and 297 days. The radial velocity measurements yield precise masses for both planets, which we use to infer their bulk heavy element content. Both planets contain approximately 30 Earth masses of heavy elements, but their bulk metallicities (i.e., the ratio between metal mass and total mass) are drastically different (0.86 ± 0.04 and 0.22 ± 0.04 respectively). Envelope mass loss cannot account for this difference due to the relatively large orbital distance and mass of the inner planet. We conclude that the outer planet underwent runaway gas accretion while the inner planet did not. This bifurcation in accretion histories is likely a result of the accretion of gas with very different metallicities by the two planets or the late formation of the inner planet from a merger of sub-Neptunes. Kepler-511 uniquely demonstrates how giant planet formation can produce strikingly different outcomes even for planets in the same system.

1. INTRODUCTION

One of the many interesting findings to come from the discovery and characterization of exoplanet systems in recent years is that multiplanet systems are common. This conclusion about planet multiplicity has been reached by transit and radial velocity (RV) alike (e.g., Thompson et al. 2018; Bryan et al. 2019; Rosenthal et al. 2021; Zhu 2022). Of multiplanet systems, those with multiple giants pose interesting questions about planetary formation and the evolution of the system as a whole. Each giant planet formed from the same protoplanetary disk, but a variety of initial conditions (e.g., Miguel et al. 2011; Öberg et al. 2011), migration chan-

nels (e.g., Goldreich & Tremaine 1980; Rasio & Ford 1996; Wu & Murray 2003; Lithwick & Naoz 2011; Winn et al. 2011), and other potentially stochastic processes (e.g., Carrera et al. 2019) eventually produce the planetary system as it is observed today. By measuring the current orbital and physical properties of giant planets in multiplanet systems, we aim to disentangle these processes and better understand planet formation as a whole.

Multiplanet systems containing transiting exoplanets are a particularly interesting subset because they allow for the measurement of at least one of the planet’s radius and thereby its bulk density. In the specific case of a giant exoplanet, the bulk composition can lend clues about the planet’s heavy element abundance (e.g., Guillot et al. 2006), which in turn informs its formation and evolution (e.g., Pollack et al. 1996; Mousis et al. 2009; Thorngren et al. 2016; Hasegawa et al. 2018). Hav-

Corresponding author: Yayaati Chachan
yayaati.chachan@mcgill.edu

* CITA National Fellow

ing this constraint for *all* of the known giant planets in a particular system is especially valuable as a tool for investigating different accretion process ongoing in the same system. According to the NASA Exoplanet Archive (Akeson et al. 2013), of the nearly 900 known multiplanet systems, well over 100 have at least one transiting giant planet but only a few dozen contain multiple giant transiting planets¹.

Recent simulations aimed at capturing the impact of disk gap formation on multiple forming giants planets have found that the diverse distribution of mass ratios between giant planets in the same system necessitates different accretion start times as well as some amount of truncation of runaway accretion by disk dispersal (Bergez-Casalou et al. 2023). Runaway accretion can occur at different times in different locations with a protostellar disk owing to different disk conditions (e.g., Ikoma et al. 2001; Bitsch et al. 2018). In this way, mass measurements of multiple giant planets in the same system provide insight into the properties of the local disk in which they both formed.

Moreover, the final orbital distances of giant planets in multiplanet systems hold clues as to how the planets migrated and initial disk properties, which is especially interesting for comparison with our own multi-giant-planet system. Griveaud et al. (2023) found that pairs of giant planets only migrate inward in low viscosity disks and end up as “warm Jupiters,” in contrast to Solar System based theories that suggest that Jupiter and Saturn also migrated outward together (e.g., Tsiganis et al. 2005; Walsh et al. 2011).

In this work, we confirm and characterize the Kepler-511 system (KOI-289), which was previously known to contain two statistically validated giant planets (Morton et al. 2016; Valizadegan et al. 2022). Despite the fact that Kepler-511 b and Kepler-511 c have long orbital periods relative to other transiting exoplanets (297 days and 27 days, respectively), both planets transit their host star. Moreover, the factor of 10 difference in their orbital periods (5x in semimajor axis), is much larger than nearly all other well characterized systems of multiple transiting giant exoplanets.

This paper is organized as follows. In Section 2, we describe transit observations of Kepler-511 from the Kepler spacecraft and follow-up spectroscopy from Keck Observatory. In Section 3, we model the stellar and planetary properties of this system with EXOFASTv2 (Eastman et al. 2019) and exoplanet (Foreman-Mackey et al. 2021a). In Section 4 we present the results of the

modeling and take a step further to estimate bulk heavy element abundance of both planets. Interestingly, both planets have similar masses of heavy elements but their bulk metallicity is notably different. In Section 5, we propose theories for how Kepler-511 b and Kepler-511 c formed given their bulk metallicities. Finally, in Section 6, we summarize our analysis and primary findings.

2. OBSERVATIONS

In the following sections, we describe how all photometric and spectroscopic observations were collected and processed.

2.1. Photometric data from Kepler

Kepler-511 was observed by the Kepler spacecraft (Borucki et al. 2010) in Quarters 0–17. We downloaded the data from the Mikulski Archive for Space Telescopes using the `lightkurve` package (Lightkurve Collaboration et al. 2018). Most of the data were acquired at long cadence (30 minutes), although some short cadence (1 minute) data were available in Quarts 6 and 7. When both types of data were available, were defaulted to using the short cadence. We made use of the Pre-search Data Conditioning Simple Aperture Photometry (PDCSAP; Jenkins et al. 2010; Smith et al. 2012; Stumpe et al. 2012) which was detrended for various systematic noise sources. The only additional detrending applied to the PDCSAP flux at this stage was a simple outlier removal. The light curves showed low frequency signals, likely due to stellar variability, but these were handled later in the modeling (Section 3). In total, Kepler observed four transits of Kepler-511 b and over 50 transits of Kepler-511 c.

The Kepler-511 system was included in the transit timing variation (TTV) analysis of Holczer et al. (2016). The average significance (i.e., measurement divided by uncertainty) of the TTVs in the transits of both planets was less than unity. As a result, we did not account for possible TTVs when modeling the ephemeris of the Kepler-511 planets.

2.2. Spectroscopic data from HIRES

We acquired 20 spectra of Kepler-511 from the W. M. Keck Observatory using the High Resolution Echelle Spectrometer (HIRES; Vogt et al. 1994) over a span of 8.5 years. 19 of these spectra were acquired with a heated I₂ cell in the light path, which imprinted a set of reference spectral lines that enabled wavelength calibration and a tracking of the instrument profile for each observation. These data were acquired with moderate signal-to-noise (S/N) values between 47 and 98. The other observation was taken without the I₂ cell and had

¹ <https://exoplanetarchive.ipac.caltech.edu>

Table 1. RV Measurements of Kepler-511 From Keck-HIRES.

BJD _{TDB}	RV (m s ⁻¹)	S_{HK}
2456449.90146	37.8 ± 3.2	0.137 ± 0.001
2456484.90839	36.3 ± 2.8	0.129 ± 0.001
2456513.84738	45.3 ± 3.0	0.128 ± 0.001
2456524.76180	21.7 ± 2.8	0.128 ± 0.001
2456532.79213	28.8 ± 2.6	0.129 ± 0.001
2457200.97212	33.1 ± 3.6	0.130 ± 0.001
2458294.92664	11.8 ± 3.4	0.137 ± 0.001
2458329.90056	-10.1 ± 3.6	0.132 ± 0.001
2458389.76351	2.9 ± 3.7	0.133 ± 0.001
2458632.87369	-18.1 ± 4.2	0.130 ± 0.001
2458714.89043	10.0 ± 3.3	0.128 ± 0.001
2458787.74592	-11.7 ± 3.8	0.122 ± 0.001
2459038.93765	8.9 ± 3.7	0.130 ± 0.001
2459099.87107	-20.2 ± 4.2	0.118 ± 0.001
2459296.13499	-19.2 ± 4.2	0.149 ± 0.001
2459421.02970	-33.1 ± 4.7	0.079 ± 0.001
2459445.99461	-41.3 ± 4.1	0.120 ± 0.001
2459470.84732	-40.0 ± 3.4	0.130 ± 0.001
2459546.76795	-45.2 ± 5.5	0.123 ± 0.001

a higher S/N (126). This spectrum was used as a template in the forward modeling procedure that yielded the precise RV corresponding to each I₂-in observation (Butler et al. 1996; Howard et al. 2010; Fulton et al. 2015). The precise RVs for Kepler-511 are listed in Table 1.

The wavelength coverage of HIRES (~360–900 nm) enables the measurement of the S_{HK} stellar activity indicator from the Ca II H and K lines (Wright et al. 2004; Isaacson & Fischer 2010). We include this indicator alongside the RVs in Table 1.

3. MODELING KEPLER-511 SYSTEM PARAMETERS

3.1. Stellar parameters

We processed the high S/N template spectrum (Section 2.2) of Kepler-511 with SpecMatch (Petigura et al. 2017) to determine its spectroscopic properties: stellar effective temperature $T_{\text{eff}} = 5585 \pm 100$ K, iron abundance $[\text{Fe}/\text{H}] = -0.36 \pm 0.06$ dex, surface gravity $\log g = 4.10 \pm 0.10$, and rotational velocity $v \sin i = 1.8 \pm 1.0$ km s⁻¹. We then treated these values of T_{eff} and $[\text{Fe}/\text{H}]$ as normal priors in an EXOFASTv2 fit between stellar evolution models and archival broadband

Table 2. Median Values and 68% Confidence Interval for Kepler-511 Stellar Parameters

Parameter	Units	Values
M_*	Mass (M_{\odot})	1.024 ^{+0.070} _{-0.060}
R_*	Radius (R_{\odot})	1.785 ^{+0.063} _{-0.061}
L_*	Luminosity (L_{\odot})	3.49 ± 0.20
F_{Bol}	Bolometric Flux (cgs)	2.66×10^{-10} ^{+1.5 × 10⁻¹¹} _{-1.4 × 10⁻¹¹}
ρ_*	Density (cgs)	0.253 ^{+0.035} _{-0.029}
$\log g$	Surface gravity (cgs)	3.945 ^{+0.044} _{-0.040}
T_{eff}	Effective Temperature (K)	5902 ⁺⁸⁸ ₋₈₆
[Fe/H]	Metallicity (dex)	-0.356 ^{+0.064} _{-0.060}
[Fe/H] ₀	Initial Metallicity ¹	-0.264 ^{+0.082} _{-0.079}
Age	Age (Gyr)	7.5 ^{+1.7} _{-1.5}
EEP	Equal Evolutionary Phase ²	456.7 ^{+3.3} _{-4.9}
A_V	V-band extinction (mag)	1.03 ^{+0.062} _{-0.066}
σ_{SED}	SED error scaling	1.49 ^{+0.59} _{-0.36}
ϖ	Parallax (mas)	1.544 ± 0.016
d	Distance (pc)	647.8 ^{+6.8} _{-6.6}

See Table 3 in Eastman et al. (2019) for a description of all parameters.

¹ The metallicity of the star at birth.

² Corresponds to static points in a star’s evolutionary history. See Dotter (2016).

photometry (Eastman et al. 2013, 2019). The SpecMatch results were not used to place a prior on $\log g$ as it is only weakly constrained by spectroscopic data and placing such a prior on it can bias fitted stellar properties (Torres et al. 2012). We point the reader to Eastman et al. (2019) for a complete description of the EXOFASTv2 stellar evolution modeling. Briefly, EXOFASTv2 interpolates a grid of MIST isochrones (Paxton et al. 2011, 2013, 2015; Dotter 2016; Choi et al. 2016) and precalculated bolometric corrections to derive basic stellar parameters and model the host star’s spectral energy distribution. Our EXOFASTv2 fit included a uniform prior on reddening ($A_V \in [0, 0.19778]$) from galactic dust maps (Schlafly & Finkbeiner 2011) and parallax ($\varpi = 1.544 \pm 0.198$ mas) from Gaia Data Release (DR) 2 (Gaia Collaboration et al. 2016, 2018). We also imposed noise floors on T_{eff} and bolometric flux consistent with the findings of Tayar et al. (2020) to avoid account for systematic uncertainties in the MIST models and to avoid overconstraining our stellar—and thereby planetary—parameters. The EXOFASTv2 fit proceeded until convergence, which was assessed for each fitted parameter using the Gelman-Rubin statistic (<1.01) and the number of independent draws from the posterior (>1000). The final stellar parameters are listed in Table 2.

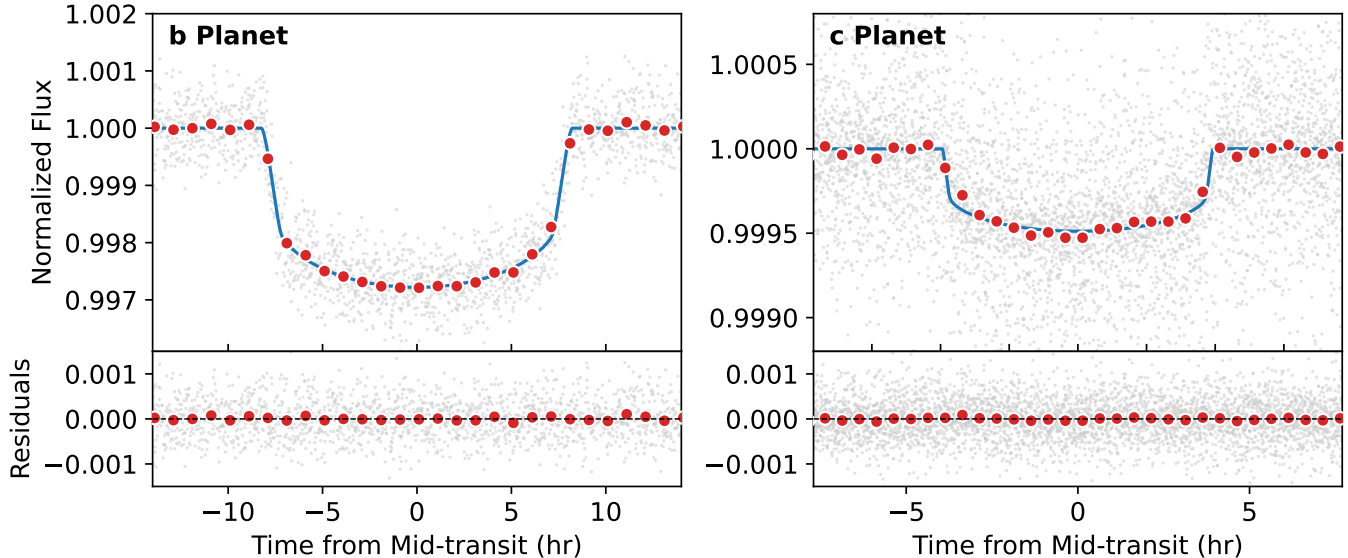


Figure 1. Kepler data and the median transit model, folded on the best fit ephemeris (Table 3), for both Kepler-511 planets. Gray points represent individual frames, and red points are 1 hour and 0.5 hour bins for Kepler-511 b and Kepler-511 c, respectively.

Kepler-511’s luminosity and inferred stellar parameters imply that it is evolving off the main sequence. The broadband photometry of Kepler-511 indicates that the star is significantly more luminous than the Sun². One potential confounding possibility for the source’s high luminosity is the presence of an unresolved companion. In fact, Kraus et al. (2016) reported a potential companion with a ΔK -band magnitude of 0.189 and a separation of $0''.017$ based on observations from NIRC2 on the Keck II telescope. Such a small K -band contrast requires the companion to be nearly equal mass and the small separation corresponds to a mere ~ 11 au in projected separation. The presence of such a binary companion would significantly complicate our ability to place constraints on the properties of the two stars and consequently any planets around them.

To resolve this issue, we closely examined various lines of evidence that support or reject the hypothesis of a nearby companion of Kepler-511. First, we note that the reported detection pushed the resolving power of the NIRC2 instrument and that the companion has not been confidently recovered in follow up imaging observations of the system (A. Kraus, private communica-

tion). This could be due to orbital motion of the companion. Second, the high-resolution template spectrum of the star obtained as part of the RV observations does not contain any hint of the presence of two stars and is well fitted by a single star template (Kolbl et al. 2015). In the unlikely scenario that the binary companion is spectroscopically unresolved, we would expect the line profiles of the source to vary with time due to stellar orbital motion. However, the χ^2 and residuals of RV spectra fits do not exhibit any meaningful variation with epoch. Third, the RV measurements of the star show a long-term trend of only ~ 77 m/s over the course of 8.5 years. The presumptive nearly-equal mass stellar companion would have to be on a highly improbable nearly face-on orbit to produce this relatively small RV trend. Such an orbit would also suggest that the companion should be detectable at other epochs, in contrast to follow up observations. All of these considerations lead us to conclude that Kepler-511 is likely a slightly-evolved single star rather than a binary. Continued RV monitoring and future direct imaging observations would shed further illumination on the nature of this system.

3.2. Planetary parameters

We used exoplanet (Foreman-Mackey et al. 2021a) to jointly model the Kepler-511 transit and RV data. We parameterized the transit models with the orbital period, the ratio between planetary and stellar radius, the stellar density, and quadratic limb darkening parameters following Kipping (2013). We used our fit to the broadband photometry of the star to place a normal

² The exact luminosity does depend on the photometric points chosen for the fit. In their large scale studies of planet-hosting stars, Berger et al. (2020) and Berger et al. (2023) chose 2MASS + SDSS g -band photometry and the Gaia G_{BP} and G_{RP} photometry for Kepler-511 and find that it is $2.75^{+0.20}_{-0.19}$ and $3.01^{+0.13}_{-0.12}$ times as luminous as the Sun, respectively. We use a wider range of photometric measurements for Kepler-511, which should provide a more reliable estimate of its stellar properties

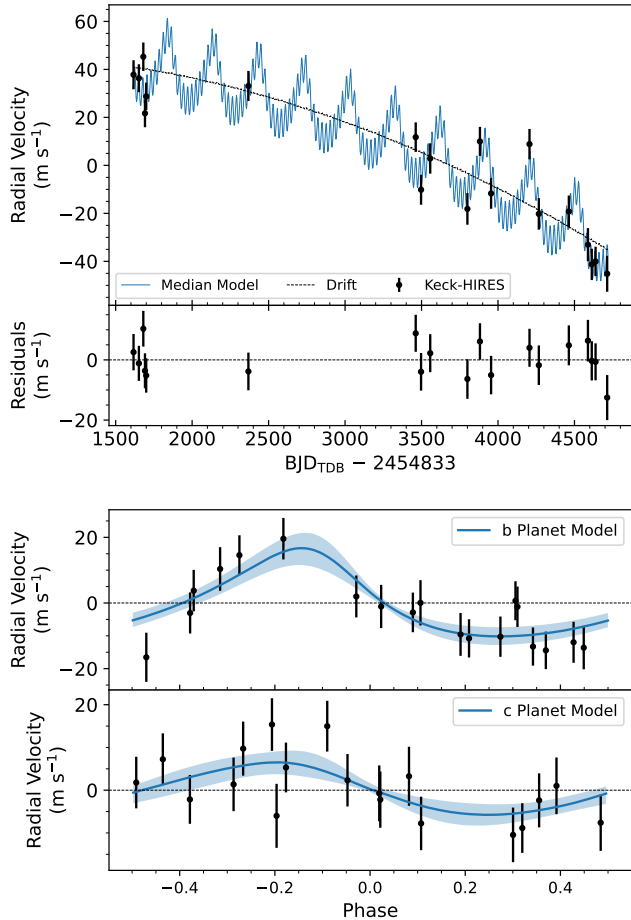


Figure 2. Top: time-series RV data from Keck-HIRES (black points) and median RV model (blue line). The need to include a long-term trend (dashed black line) in addition to the two planetary Keplerian signals is evident. Bottom: individual components of the RV for each planet folded on the best fit ephemeris such that a phase of zero is the conjunction time (Table 2). The blue lines are the median models and the blue shaded regions are the 68% confidence intervals.

prior on the stellar density (Table 2) in our transit fit. A fit without a prior on the stellar density produced a higher likelihood ($\Delta\text{BIC} = 14$) and higher stellar density that only agrees with the SED fitted value at the 2σ level. However, this difference in likelihood is driven entirely by the small number of RV data points, which biases the stellar density to higher values. The normal prior on stellar density is therefore placed to alleviate this issue, in line with previous studies (Espinoza et al. 2019). The transit model also included a quasiperiodic Gaussian Process (GP) meant to model the stellar variability signal in the photometry (e.g., Angus et al. 2018). The kernel of the GP took the form of an overdamped stochastic harmonic oscillator. The short and long cadence data were treated with separate GP models. For

the RV model, we included terms for a quadratic trend, which were necessary based upon inspection of the time-series data (Figure 2).

The exoplanet fit proceeded in two parts. First, there was an optimization of the fitted parameters to identify the local maximum a posteriori (MAP) point of the model. This MAP model included the GP for the photometry. We ran the MAP model several times, adjusting the starting points of the parameters and the order in which the parameters were optimized. Each time, we visually inspected the residuals with the transit and RV data until we were satisfied that the MAP solution was representative of the transit and RV data. We derived the photometric variation caused by stellar variability from this optimization and subtracted it from the transit light curves to effectively flatten the photometry.

Second, we launched a Markov Chain Monte Carlo (MCMC) routine to generate posterior predictive samples from the joint transit and RV model using the flattened photometry. The MCMC proceeded with 1,500 tuning steps before making 6,000 draws of the posterior. At that point, each fitted parameter had a Gelman-Rubin statistic of <1.01 and an effective sample size of $\gtrsim 1,000$, which we took to demonstrate convergence.

The median transit models, folded on the ephemeris of each planet, are shown in Figure 1. The median and 68% confidence interval of the RV model are shown in Figure 2. The fitted parameters along with a few informative derived parameters are listed in Table 3. In deriving physical parameters from relative ones, we used the stellar properties and uncertainties listed in Table 2.

3.3. A distant companion in Kepler-511 system?

Possibly adding to the peculiarity of the Kepler-511 system is the presence of a large RV drift (~ 77 m/s) present over the 8.5 year observational baseline (Figure 2). This RV trend is unlikely to be due to stellar activity as its amplitude is larger than what one might expect from the activity (e.g., Lovis et al. 2011) and because there is little correlation (Pearson correlation coefficient of 0.35) between the RVs and the S_{HK} values measured from the Ca II H and K lines for the Keck-HIRES RVs (Table 1) (e.g., Díaz et al. 2016; Butler et al. 2017; Rosenthal et al. 2021).

The most plausible hypothesis for the cause of this trend is a distant companion orbiting far beyond Kepler-511 b. Such a companion would have important implications for the formation of the entire system, as planet-star and planet-planet interaction alike can excite eccentricity of inner planets (e.g., Wu & Murray 2003;

Table 3. Median Values and 68% Confidence Interval for the Kepler-511 Planet Parameters

Parameter	Units	Values	
		Kepler-511 b	Kepler-511 c
P	Period (days)	296.63766 ± 0.00039	26.629424 ± 0.000039
R_p	Radius (R_J)	0.886 ± 0.033	$0.371^{+0.018}_{-0.017}$
M_p	Mass (M_J)	$0.44^{+0.11}_{-0.12}$	$0.100^{+0.036}_{-0.039}$
T_C	Time of Conjunction (BJD _{TDB})	$2455236.67214^{+0.00083}_{-0.00082}$	2454971.7374 ± 0.0013
a	Semi-major Axis (au)	0.894 ± 0.048	0.1792 ± 0.0097
i	Inclination (degrees)	$89.719^{+0.029}_{-0.037}$	$88.59^{+0.38}_{-0.75}$
e	Eccentricity	$0.277^{+0.070}_{-0.068}$	$0.17^{+0.14}_{-0.11}$
ω_*	Argument of Periastron (degrees)	26^{+19}_{-13}	18^{+89}_{-95}
T_{eq}	Equilibrium Temperature ¹ (K)	402 ± 14	899 ± 32
K	RV Semi-amplitude (m s^{-1})	$13.7^{+3.4}_{-3.8}$	$6.8^{+2.4}_{-2.6}$
R_p/R_*	Radius of Planet in Stellar Radii	$0.04986^{+0.00054}_{-0.00056}$	$0.02089^{+0.00066}_{-0.00061}$
a/R_*	Semi-major Axis in Stellar Radii	107.6 ± 4.4	21.57 ± 0.89
δ	Transit Depth ($(R_p/R_*)^2$)	$0.002486^{+0.000054}_{-0.000056}$	$0.000436^{+0.000028}_{-0.000025}$
b	Transit Impact Parameter	$0.527^{+0.049}_{-0.066}$	$0.53^{+0.14}_{-0.28}$
ρ_p	Density (g cm^{-3})	$0.84^{+0.23}_{-0.25}$	$2.6^{+1.0}_{-1.1}$
S_p	Insolation (S_\oplus)	4.37 ± 0.54	109 ± 13
Kepler Limb-darkening Parameters:			
u_1	Linear Coefficient		$0.524^{+0.097}_{-0.085}$
u_2	Quadratic Coefficient		$0.02^{+0.13}_{-0.14}$
Keck-HIRES Parameters:			
γ	Relative RV Offset ² (m s^{-1})		$14.13^{+0.94}_{-0.96}$
$\dot{\gamma}$	RV Linear Trend Coefficient ² ($\text{m s}^{-1} \text{d}^{-1}$)		$-0.0246^{+0.0015}_{-0.0014}$
$\ddot{\gamma}$	RV Quadratic Trend Coefficient ² ($\text{m s}^{-1} \text{d}^{-2}$)		$-0.0000047^{+0.0000012}_{-0.0000013}$
σ_J	RV Jitter (m s^{-1})		$5.1^{+1.8}_{-1.4}$
Kepler Nuisance Parameters:			
		Short Cadence	Long Cadence
σ_F^2	Added Flux Variance	$0.0004654^{+0.0000041}_{-0.0000040}$	0.0000956 ± 0.0000016
F_0	Baseline Flux	1.0000 ± 0.0060	0.9999 ± 0.0029

¹ Assumes no albedo and perfect redistribution.² Relative to time BJD_{TDB} = 2457998.3347095.

Lithwick & Naoz 2011). A direct imaging campaign with the NIRC2 instrument on the Keck II telescope that targeted Kepler-511 for resolved stellar companions claimed two detections (Kraus et al. 2016; Furlan et al. 2017): the first with a ΔK -band magnitude of 0.189 and separation of $0''.017$, and the second with a ΔK -band magnitude of 7.796 and separation of $3''.26$. Recent Gaia astrometry identifies the $3''.26$ companion as Gaia DR 3 2107644188495101440, which is clearly not bound to Kepler-511 based on proper motion (Gaia Collaboration et al. 2022). We discussed the possibility that the closer companion is potentially a false positive in Section 3.1. Such a small K -band contrast would imply that this purported companion is nearly equal mass as the primary star and require the companion to be on a

highly improbable face-on orbit to produce the observed RV trend.

The RV drift shows significant curvature (the quadratic trend coefficient is non-zero at $\sim 4\sigma$ level), possibly suggesting that the observations sampled a portion of the distant companion's orbit near quadrature and allowing us to draw useful constraints on the distant companion's properties. We put constraints on the companion properties by subtracting the best fit solutions for planets b and c from the RV data and fitting the residual long-term trend with RadVel. This procedure does not allow us to account for the covariance between properties of the transiting planets and the distant companion. However, given the limited number of RV measurements, a three planet fit is unfeasible due to

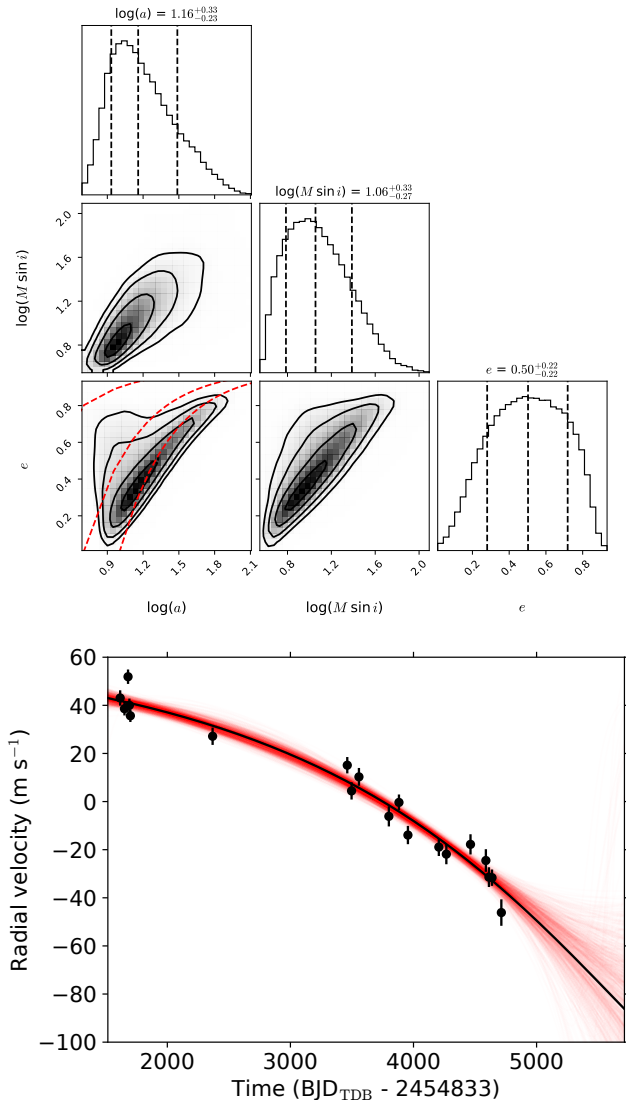


Figure 3. Top: Corner plot for the constraints on the semi-major axis (AU), $M \sin i$ (M_{Jup}), and eccentricity of the distant companion. The red dashed lines in the eccentricity - semimajor axis 2D histogram mark pericenter values of 1, 5, and 10 au. Bottom: Black points mark the RV data with the best fit model for the two transiting planets subtracted out. The black curve shows the best fit model to the long term trend and the red curves correspond to 1000 models from randomly drawn parameters from the posterior.

the large number of free parameters. Our constraints on the distant companion are likely to be tighter than the data merit but still useful for gauging the companion’s properties and guiding follow up RV campaigns. The top panel of Figure 3 shows the posteriors for the distant companion’s semi-major axis, minimum mass ($M \sin i$), and eccentricity. The RV trend, best fitting model, and 1000 sample models are shown in the bottom panel of Figure 3.

The distant companion in the Kepler-511 system may be planetary or stellar in nature. Given that we sample its orbit only partially, our constraints on its semi-major axis, mass, and eccentricity are highly correlated. Combinations of eccentricity and semi-major axis that lead to pericenter values (1, 5, and 10 au marked with red dashed lines in top panel of Figure 3) close to the inner planets’ orbits are implausible as they would violate the long-term stability of the system. These constraints also confirm our earlier analysis regarding the plausibility of a nearly equal mass stellar companion around Kepler-511: it would need to be on a nearly face on orbit to match the observed RV trend. The distant companion is more likely to be a sub-stellar object or a very low mass star on an eccentric orbit with a semi-major axis of $\sim 10 - 100$ au. Continued RV follow up would be extremely useful for characterizing the properties of this companion and for understanding the context in which the inner planets formed and evolved.

4. THE KEPLER-511 PLANETS

Based upon the aforementioned photometric and spectroscopic data acquired of the Kepler-511 system, we find that Kepler-511 b and Kepler-511 c both have masses well within the planetary regime, thereby dynamically confirming them as genuine exoplanets. Figure 4 shows planets b and c in context with other planets that have measured masses and radii. Kepler-511 b joins the small but growing group of transiting cool giant exoplanets on orbits longer than ~ 100 days with precisely measured masses (e.g., Dalba et al. 2021a). Kepler-511 c presents as a dense Neptune-sized planet that may have a considerable gas envelope, just based on its mass and radius.

Amongst multi-planet systems, the Kepler-511 system is unique in that Kepler-511 c is significantly more massive than the inner super-Earths that typically accompany cold giants (e.g., Zhu & Wu 2018; Bryan et al. 2019). Since the ability of planetary cores to accrete gas depends strongly on their mass, one would expect Kepler-511 c to be gas rich. Instead, Kepler-511 c is much smaller in size than planets of comparable mass in this sample, indicating that it is not as gas rich as other similar mass planets that accompany outer giants. The combination of these contradictory properties makes the Kepler-511 system interesting from a planet formation perspective. To explore the formation scenarios for the Kepler-511 planets further, we quantified the bulk heavy element content of both planets.

4.1. Planetary bulk metallicity

With a known mass, radius, and age for each planet in the Kepler-511 system, we retrieved the total mass

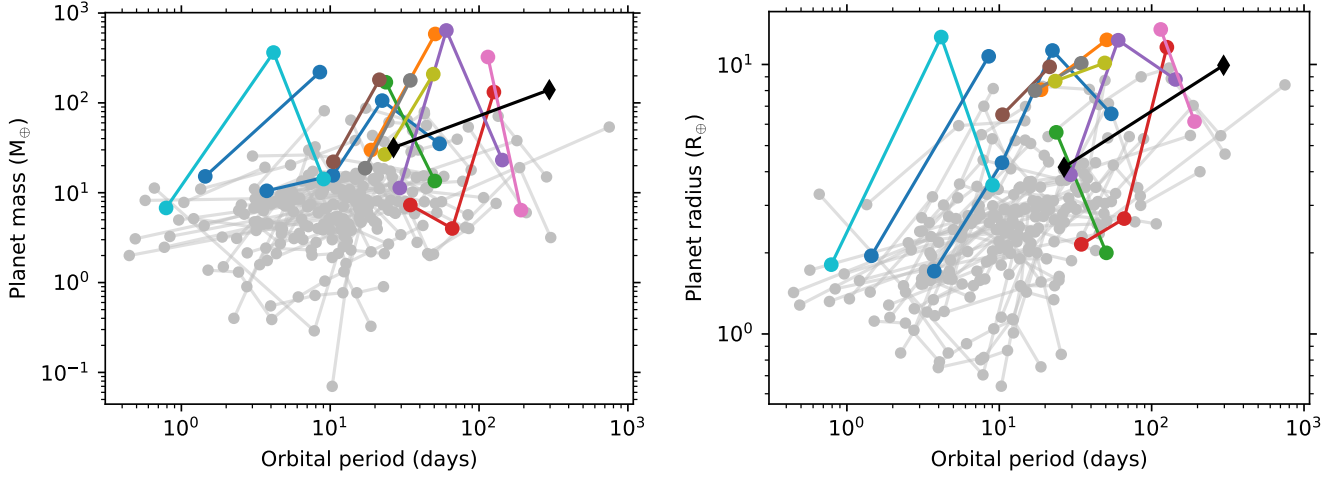


Figure 4. Multi-planet systems with planets that have measurements for both their masses (left) and radii (right) are shown (data from the exoplanet archive). Systems that do not have a single planet with mass $> 95M_{\oplus}$ are grayed out. The Kepler-511 planets are shown with black diamonds. Kepler-511 b is the longest orbital period planet in such a sample. Gas rich giants ($> 95M_{\oplus}$) are typically accompanied by planets that are significantly less massive than Kepler-Kepler-511 c. Some planets that do have masses similar to Kepler-511 c are typically much larger than it, indicating that they are much more gas rich compared to Kepler-511 c.

of heavy elements that are possibly present within these planets (i.e., their bulk metal mass M_Z). We use a 1D planetary evolution model coupled to a radiative atmosphere model in order to evolve the radius of a giant planet along its cooling curve at a given mass. At the age of the system, we adjust M_Z to retrieve the known radius. Additional details of this method and the models and assumptions used are reported by [Thorngren et al. \(2016\)](#) and [Thorngren & Fortney \(2019\)](#).

We found that the bulk metallicities ($Z_p \equiv M_Z/M_p$) of Kepler-511 b and c are 0.22 ± 0.04 ($Z_p/Z_{\star} = 35 \pm 8$) and 0.86 ± 0.04 ($Z_p/Z_{\star} = 137 \pm 20$), respectively. Figure 5 shows the posteriors distributions for these metal retrievals and demonstrates that the fits are converged and lack strong correlations between parameters. Both planets are above the average of, although still consistent with, the correlation between relative bulk metallicity and giant planet mass identified by [Thorngren et al. \(2016\)](#).

The measured bulk metallicities imply remarkably similar amounts ($30 \pm 9 M_{\oplus}$ and $28 \pm 10 M_{\oplus}$ respectively) of heavy elements in planets b and c despite the fact that they differ in mass by a factor of ~ 4.5 . This difference could suggest that Kepler-511 b experienced runaway gas accretion while Kepler-511 c did not. Such a scenario is peculiar given that ability of a planet to accrete gas is strongly dependent on the amount of heavy elements it contains. Despite having similar amounts of heavy elements, these planets have very different gas contents. This makes the Kepler-511 planets invaluable

for studying giant planet formation history and gauging the role of other properties that control gas accretion.

It is interesting that two metal enriched giant planets formed around such a metal-poor host star ($[Fe/H] = -0.36$) given the observed correlation between stellar metallicity and giant planet occurrence (e.g., [Fischer & Valenti 2005](#)). The combined metal mass in the two planets stretches the initial disk mass one needs for their formation around such a low metallicity star. Assuming i) a 100% efficiency of converting dust to these planetary cores, ii) the disk has the same metallicity as the host star, and iii) a dust to gas mass ratio of 0.01 for a solar metallicity star, one would require a gas disk that is at least 3.8% the mass of the host star to have $58 M_{\oplus}$ of dust mass. Given that efficiency of converting dust to planets is likely much smaller than 100% and this estimate does not include the mass contained within the distant companion, the protostellar disk around Kepler-511 must have been $\gtrsim 20\%$ of the mass of the host star. In the following section, we will consider how various theories of giant planet formation can explain the inferred bulk metallicities for the Kepler-511 planets.

5. FORMATION AND EVOLUTION HISTORIES OF THE KEPLER-511 PLANETS

The planets in the Kepler-511 system demonstrate the benefit of measuring precise masses and making bulk composition assessments for cool, giant exoplanets. Having only validated these planets (i.e., only measured their radii), our interpretation was limited to the fact that Kepler-511 is a system of multiple giant planets. By

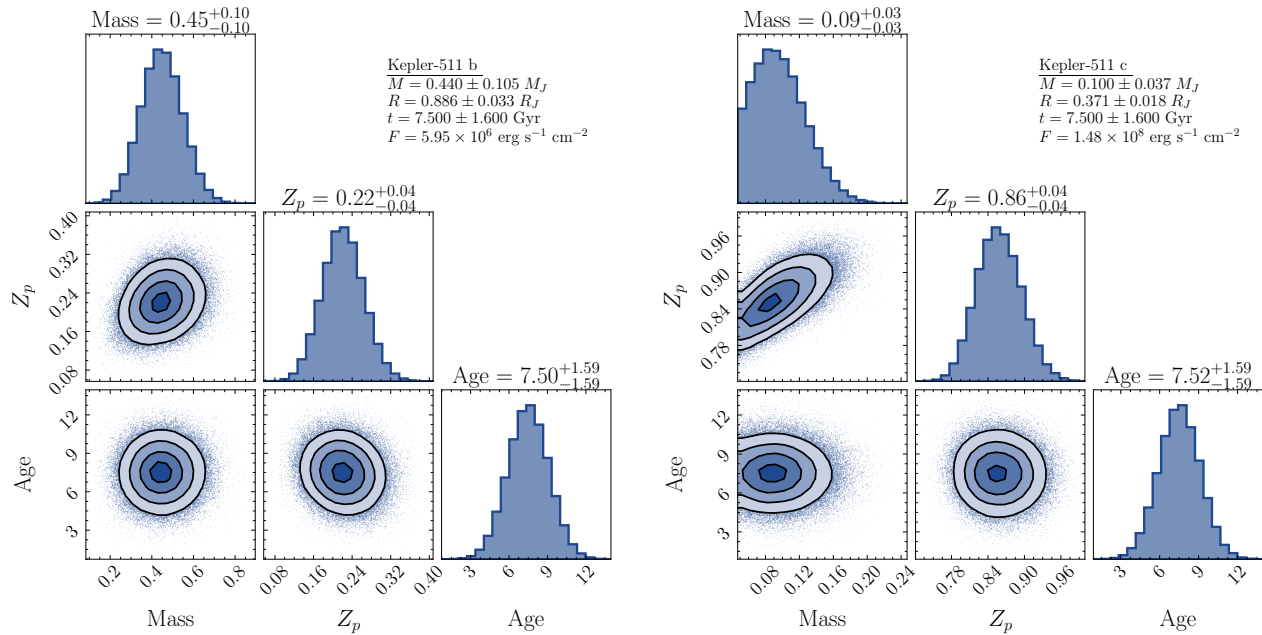


Figure 5. Posterior probability distributions for bulk metallicity (Z_p) retrievals for Kepler-511 b (left) and Kepler-511 c (right). In both cases, the inferred values of Z_p do not show significant correlations with the measured planet masses or system age. By mass, Kepler-511 b and Kepler-511 c are 22% and 86% heavy elements.

measuring masses and inferring their bulk metallicities, we can now conclude that these two sibling planets underwent different accretion processes during formation. In the following sections, we consider three broad explanations for how Kepler-511 b and Kepler-511 c formed and why they are so different from each other.

5.1. Envelope mass loss history

As the first explanation for the large composition difference between Kepler-511 b and c, we consider whether XUV-driven mass loss could have removed a substantial portion of the inner planet’s envelope. Considering the XUV mass loss models of Lopez et al. (2012, their Figure 5), a planet with a bulk density of 2.7 g cm^{-3} and receiving an irradiation of $\sim 110 S_{\oplus}$ should experience negligible mass loss on the order of $0.1 M_{\oplus}$ per Gyr (0.3% of Kepler-511 c’s current total mass per Gyr). To verify and refine this approximate result, we applied the models of Thorngren et al. (2023) to Kepler-511 c. These models simulate the thermal and mass-loss evolution of giant planets using the stellar XUV evolution tracks of Johnstone et al. (2021) and the XUV-driven mass-loss models of Caldiroli et al. (2022).

For the planet’s structure, we adopt a core mass of $10 M_{\oplus}$ and adjust the envelope metallicity to 0.81 to match the observed radius (for a total $Z = 0.87$). Evolving forward from $0.101 M_J$, we estimate that the planet has lost just $0.194 M_{\oplus}$ of envelope material (0.67% of Kepler-511 c’s current total mass) over its ~ 7.5 Gyr.

lifetime. We find an insignificant present-day mass loss rate of approximately $0.00906 M_{\oplus} \text{ Gyr}^{-1}$ (0.03% of Kepler-511 c’s current total mass). The estimates of mass loss are insensitive to the adopted core mass since the envelope metallicity will have to be adjusted accordingly to match the radius. For example, using a $25 M_{\oplus}$ core results in the loss of $0.188 M_{\oplus}$ over the planet’s life. While the rate of mass loss may vary somewhat based on how active the star was in its early life (most of the mass-loss occurs in the first couple Gyr.), there is not a plausible value that would lead to substantial mass loss – the planet is simply too massive and distant from its parent star.

5.2. Differing envelope accretion histories

The accretion of primordial envelopes is controlled by the mass of the planetary core, the metal content of the accreted gas, and to a lesser extent, the ambient nebular conditions (Stevenson 1982; Rafikov 2006; Lee et al. 2014; Piso et al. 2015). Given the remarkable similarities in the total metal content of the two planets, it is reasonable to first assume that the two planets had cores of similar masses. If the two cores are assumed to be $28 M_{\oplus}$ each, can differences in accreted material or nebular conditions account for their differing final masses and bulk densities? For this scenario to be plausible, Kepler-511 b must attain a gas-to-core mass ratio (GCR) of > 0.5 and subsequently undergo runaway ac-

cretion while Kepler-511 c only reaches a GCR of $\sim 1/6$ before the dissipation of the protoplanetary disk.

This difference is unlikely to be driven by differences in ambient gas density at the location of the two planets. The gas density at Kepler-511 c’s location would need to be a factor of $\sim 10^4$ lower compared to the density at Kepler-511 b’s location, which would require Kepler-511 c’s $28 M_{\oplus}$ core to assemble only as the gas begins dissipating, which is similar to the merger scenario considered in § 5.3. Gap opening is also unlikely to be effective at creating such large gas density contrasts (assuming $M_p = 28 M_{\oplus}$, the gap depths would only differ by an order of magnitude for a factor of two difference in the disk aspect ratio, Duffell & MacFadyen 2013; Fung et al. 2014). We therefore focus on the formation of the Kepler-511 planets assuming accretion of material with different dust content. The accretion of gas is mediated by the cooling of the planet’s envelope (Lee & Chiang 2015), which in turn depends on the opacity at the innermost radiative-convective boundary (RCB) of the envelope. The innermost RCB of envelopes that have even a small amount of dust ($\gtrsim 0.01$ solar metallicity for ISM-like size distribution) is set by the hydrogen dissociation front, inside which H^- opacity dominates. Metallic species accreted by a planet are the primary source of free electrons that create H^- ions, and a large difference in the local disk metallicity (as can be probed with dust content) could therefore produce the divergent accretion histories of the Kepler-511 planets (Chachan et al. 2021).

Assuming both planets reached these GCRs in the same amount of time and that the temperature and the adiabatic index at their RCBs did not differ, we arrive at the following expression from Lee & Connors (2021):

$$\left(\frac{\Sigma_b}{\Sigma_c}\right)^{0.12} \left(\frac{Z_c}{Z_b}\right)^{0.4} \left(\frac{\mu_b}{\mu_c}\right)^{3.4} \gtrsim \frac{1/2}{1/6}, \quad (1)$$

where Σ is the gas surface density, Z is the dust-to-gas ratio or equivalently the dust content of the accreted material, μ is the mean molecular weight, and the subscripts correspond to the two planets. For $\Sigma \propto r^{-1}$, the ratio $\Sigma_b/\Sigma_c = a_c/a_b$, i.e. the inverse ratio of their semi-major axes. Since $1/\mu = \mu_Z/Z + \mu_{H,He}/(1-Z)$, this expression provides us with a preliminary estimate of the difference in Z required for Kepler-511 b to undergo runaway gas accretion while Kepler-511 c accretes a modest envelope.

The dust content that leads to the different formation outcomes for the Kepler-511 planets is marked in color in Figure 6. We estimate the time required for Kepler-511 c to reach a GCR of $1/6$ assuming $\Sigma_c = 2000 \text{ g cm}^{-3}$, adiabatic index of 0.17 and temperature of 2500

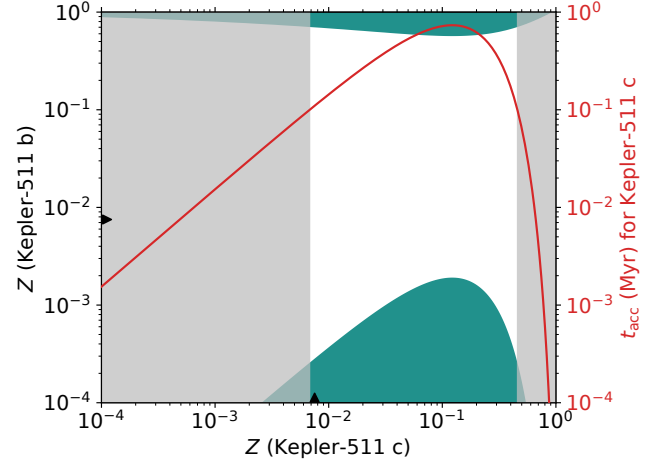


Figure 6. Bulk metallicity parameter space for Kepler-511 b (y-axis) and Kepler-511 c (x-axis). On both axes, the stellar metallicity is shown with the black triangles. The solid red line (corresponding to the right-side y-axis) shows the time (t_{acc} for Kepler-511 c to accrete its GCR of $\sim 1/6$). Grayed-out regions exclude scenarios whereby Kepler-511 c has $t_{\text{acc}} < 0.1$ Myr, which would require fine-tuning to prevent it from undergoing runaway gas accretion. The allowed regions of parameter space (green) suggest that Kepler-511 c accreted material with a higher metallicity than the host star. The metallicity of the material accreted by Kepler-511 b is likely lower than that of the host star, as the higher metallicity region is unrealistic.

K at the RCB, and the planet’s effective accretion radius to be 20% of its Hill radius. We grey out the parameter space in which Kepler-511 c accretes its envelope in less than 0.1 Myr to alleviate the issue of fine tuning the gas dissipation timescale. Figure 6 shows that for Kepler-511 c, the dust content of the material accreted must be above the stellar value to sufficiently suppress gas accretion. For Kepler-511 b, the metallicity must either be much lower to speed up envelope cooling and accretion or so much higher that the high mean molecular weight of the accreted material expedites gas accretion. The high- Z_p region for Kepler-511 b can likely be ruled out because it is unrealistically high (> 0.5).

The combination of high- Z for the inner Kepler-511 c and low- Z for the outer Kepler-511 b may be achieved if the two planets were separated by the water snowline. This scenario has the caveat that the fragmentation velocities of ice-free grains need to be smaller than those of the icy grains, such that the smaller ice-free grains slow their radial drift and pile up in the inner disk, boosting the local Z there (Chachan et al. 2021). However, latest laboratory measurements suggest the material strength between these two types of grains may be more similar than previously thought (e.g., Gundlach et al. 2018; Musiolik & Wurm 2019; Kimura et al. 2020). Alternative

mechanisms to alter the envelope opacity would require enhanced dust accretion onto Kepler-511 c due to the presence of disk substructures (e.g., [Chen et al. 2020](#)) or grain growth and expedited cooling in Kepler-511 b’s atmosphere (e.g., [Ormel 2014](#); [Piso et al. 2015](#)) to explain the different gas accretion histories for Kepler-511 b and c.

We briefly note that meridional flows that advect disk material within a planet’s Hill sphere could limit its envelope’s ability to cool and grow ([Ormel et al. 2015](#); [Ali-Dib et al. 2020](#); [Moldenhauer et al. 2021](#)). Studies that employ more realistic opacities and equations of state show that the effect of this recycling on envelope accretion is not as potent as initially supposed ([Zhu et al. 2021](#); [Bailey & Zhu 2023](#); [Savignac & Lee 2023](#)). The effect of recycling is also distance-dependent: in hotter regions of the disk close-in to the star, it can lead to a slowdown in gas accretion but the exact magnitude of the effect depends on the inner disk conditions ([Bailey & Zhu 2023](#); [Savignac & Lee 2023](#)). However, although these uncertainties might affect the amount of gas accreted by super-Earth mass cores, they are unlikely to prevent a $\sim 28 M_{\oplus}$ from accreting substantially more gas than Kepler-511 c possesses.

5.3. Kepler-511 c’s formation by giant impacts of sub-Neptunes

Since the two Kepler-511 planets have puzzling different accretion histories, we explore if this is an outcome of Kepler-511 c forming by mergers of two or three planets (sub-Neptunes) after the gas disk’s dispersal. It is more plausible that lower mass sub-Neptunes, rather than a $30 M_{\oplus}$ core, would accrete envelopes that are only $\sim 10\%$ of their mass. If these sub-Neptunes subsequently undergo a dynamical instability that leads to their coalescence into a planet such as Kepler-511 c, we could explain why Kepler-511 b turned into a gas giant while Kepler-511 c did not. This is similar to the hypothesis of late-stage formation of super-Earths ([Lee & Chiang 2016](#); [Dawson et al. 2016](#)), except we primarily consider dynamical instabilities after gas dissipation when damping by the gas does not act to stabilize the system. Such an explanation would also have the advantage of forming Kepler-511 c from inner planets that are akin to those observed around Sun-like stars, especially those interior to cold-Jupiters ([Zhu & Wu 2018](#); [Bryan et al. 2019](#)). Given the age of the Kepler-511 system ($7.5^{+1.7}_{-1.5}$ Gyr), it is plausible that a typical inner system of sub-Neptunes became unstable and merged to form Kepler-511 c. An instability might arise if the eccentricities and/or mutual inclinations of the sub-Neptunes are excited to large enough values to lead to orbit crossing.

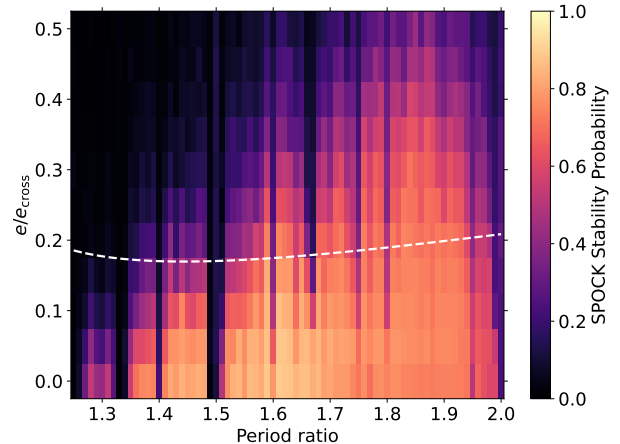


Figure 7. The stability probability for a system of three $10.5 M_{\oplus}$ planets with a given eccentricity (as a fraction of the crossing eccentricity) and period ratio accompanied by an outer giant with the properties of Kepler-511 b calculated by SPOCK. The dashed line indicates the rms time-averaged eccentricity of the three planets as a result of their interaction with the outer giant calculated via secular analytical theory.

These excitations may be a result of the planets’ mutual interactions with each other or they may be driven by the outer Kepler-511 b.

What causes instability in a tightly-packed system of planets is an area of ongoing research. In general, the onset of chaos is attributed to the overlap of two-body mean-motion resonances and three-body resonances ([Wisdom 1980](#); [Hadden & Lithwick 2018](#); [Petit et al. 2020](#); [Lammers et al. 2024](#)). The time required for a tightly-packed chain of sub-Neptunes to undergo mergers is exponentially sensitive to the orbital spacing between the planets, their orbital eccentricities, and their mutual inclinations ([Pu & Wu 2015](#)). Since the mergers are typically pairwise, it is difficult to conceive of more than two or three planets all merging together to form Kepler-511 c. Therefore, we restrict our discussion to a system of three $10.5 M_{\oplus}$ sub-Neptunes. The extent to which Kepler-511 b can excite the inner planets’ eccentricities and/or inclinations depends on the strength of their dynamical coupling, quantified by $\bar{\epsilon}$ as the ratio of the differential precession frequency of the inner planets with the outer giant and the mutual precession frequencies of the inner planets ([Pu & Lai 2018](#)). We find that for period ratios \mathcal{P} in the range of $1.2 - 2$ for the inner sub-Neptunes, $\bar{\epsilon}$ varies from $10^{-3} - 10^{-1}$. This implies that the inner sub-Neptunes would be more strongly coupled to each other than the outer giant and the giant planet alone is unlikely to drive the system to instability. Nonetheless, interactions with the outer giant planet can impart non-zero eccentricity to the inner

sub-Neptunes and we use secular perturbation theory to calculate it (Pu & Lai 2018). The rms time-averaged eccentricity of the three sub-Neptunes normalized by the crossing eccentricity ($e_{\text{cross}} = (\mathcal{P}^{2/3} - 1)/(\mathcal{P}^{2/3} + 1)$) is shown in dashed white line as a function of the period ratio \mathcal{P} of the three sub-Neptunes in Figure 7.

We use SPOCK to determine the probability that a system of three sub-Neptunes with an outer giant planet is stable over timescales of 10^9 orbits (Tamayo et al. 2020). SPOCK uses REBOUND (Rein & Liu 2012) to integrate orbits of an input planet configuration over the first 10^4 orbits and measures summary statistics that are then used to predict stability probability from a machine-learning model trained on a set of $\sim 100,000$ scale-invariant simulations of 3-planet systems. Tamayo et al. (2020) and Sobski & Millholland (2023) have shown that SPOCK generalizes well to planet configurations it was not trained on and that it agrees with prior stability metrics. We therefore adopt it to evaluate whether Kepler-511 c could have formed from mergers of a system of inner sub-Neptunes.

Period ratios \mathcal{P} of the inner sub-Neptunes are incremented by 0.01 in the range 1.25–2 and their eccentricities are set as a fraction of the orbit-crossing eccentricity (in increments of 0.05 in the range 0–0.5). For each combination of \mathcal{P} and e , we calculate the stability probability for 100 different realizations of the arguments of pericenter and the initial mean anomalies (each randomly sampled from a $\mathcal{U}[0, 2\pi)$) and average them to obtain a mean estimate that is shown by color in Figure 7. The stability probability is lowest for \mathcal{P} that correspond to integer ratios, as expected from the near-resonant interactions of the inner sub-Neptunes. Higher eccentricities also lower the probability that the system is unstable over long timescales. Eccentricity pumping due to secular interactions with Kepler-511 b therefore makes mergers of the inner sub-Neptunes more likely.

If the sub-Neptune progenitors were close to a mean-motion resonance, they would easily undergo the mergers necessary to produce a planet such as Kepler-511 c. For \mathcal{P} not close to mean-motion resonances, the stability probability can be as high as 0.4–0.8 even when planet eccentricities are set by secular perturbation from Kepler-511 b. We note that 10^9 orbits of the innermost planet only correspond to ~ 70 Myr, which is a mere 1% of the system age. These stability probabilities should be treated as upper limits and they could be much lower over Gyr timescales (10^{11} orbits). Indeed, the median and 84th percentile instability times for orbital configurations with stability probability > 0.4 (when e is set by Kepler-511 b, dashed line in Figure 7) are lower than the age of the system (Cranmer et al. 2021). Mergers there-

fore provide a plausible albeit a low likelihood pathway for the formation of Kepler-511 c like planets in some planetary systems, which would be commensurate with their low occurrence rates.

The process by which Kepler-511 b came to acquire its significant eccentricity also might have played a role in destabilizing any inner planets that could coalesce to form Kepler-511 c. For example, if the outer unconfirmed companion scattered Kepler-511 b to its current orbit, such an event could have destabilized an inner system of sub-Neptunes. A more precise measurement of Kepler-511 c’s eccentricity (our current estimate is consistent with zero) could provide more insight into its dynamical history and the plausibility of mergers as an origin channel for planets like Kepler-511 c.

6. SUMMARY

In this work, we collected RV measurements of Kepler-511 over an 8.5-year baseline (Figure 2) to dynamically confirm its two (previously validated) transiting exoplanets. Kepler-511 b is a gas giant planet with $M_p = 0.44 M_J$ on a 297 day, moderately eccentric orbit. Given its unlikely transiting orbit, Kepler-511 b is a prime member of the Giant Outer Transiting Exoplanet Mass (GOT ‘EM) survey (Dalba et al. 2021a,b; Mann et al. 2023). Its inner ($P = 27$ days) companion (Kepler-511 c) has a mass of $32 M_{\text{earth}}$ and is three times as dense. We also identify a long-term trend in the RV time series data that is most likely indicative of an additional massive object (planetary or otherwise) in the outer reaches of the Kepler-511 system (Section 3.3).

We take advantage of both planets’ relatively long orbits and low stellar irradiation (compared to other transiting exoplanets) to infer their bulk metallicities (Section 4.1). Interestingly, both planets have similar masses of heavy elements ($\sim 30 M_{\oplus}$) but only Kepler-511 b seems to have accreted a massive gaseous envelope. Since the ability of planets to accrete primordial gas depends on their heavy element content, the Kepler-511 planets are an intriguing duo that pose an informative challenge to planet formation and evolution theories.

We explore three scenarios that could account for the planets’ current properties. Firstly, we rule out envelope mass loss as a means to explaining the difference in bulk metallicities of these planets: at 27 days, Kepler-511 c is simply too far away from its host star to suffer significant mass loss. Secondly, we evaluate a variety of reasons why their gas accretion histories might have differed. Although differences in the dust content of the disk gas accreted by these planets could drive their divergent accretion histories, it is difficult to attain such strong contrasts in the local dust content. Finally, we

consider the scenario that Kepler-511 c is gas-poor because it formed from the merger of lower mass cores (that accrete less gas) after the dissipation of the protoplanetary disk. We show that secular perturbations from Kepler-511 b could pump up the eccentricities of such an inner system of sub-Neptunes and render their merger more likely over long timescales.

Overall, the Kepler-511 system serves as an important benchmark for numerous reasons. It contains multiple giant planets; both planets transit, enabling a measurement of their radii; the outer planet has an exceptionally long orbital period considering its transiting geometry, leaving it with an irradiation only 4.5 times that of the Earth and an equilibrium temperature of ~ 400 K; and the two planets seem to have divergent accretion histories. We encourage additional theoretical explorations to provide an explanation for how systems of multiple giant planets like Kepler-511 could have formed.

ACKNOWLEDGMENTS

The authors recognize the cultural significance and sanctity that the summit of Maunakea has within the indigenous Hawaiian community. We are deeply grateful to have the opportunity to conduct observations from this mountain. We acknowledge the impact of our presence there and the ongoing efforts to preserve this special place.

The authors thank all of the observers in the California Planet Search team for their many hours of hard work in collecting the RVs published here. The authors thank Jonathan Fortney, Sarah Millholland, and Yanqin Wu for helpful conversations about this planetary system. We are particularly grateful to Adam Kraus for an enlightening and extremely useful exchange on the possible binarity of this system. Part of this research was conducted at the Other Worlds Laboratory Summer Program 2022 at UC Santa Cruz, which is generously supported by the Heising-Simons Foundation. P.D. acknowledges support by a 51 Pegasi b Postdoctoral Fellowship from the Heising-Simons Foundation and by a National Science Foundation (NSF) Astronomy and Astrophysics Postdoctoral Fellowship under award AST-

1903811. M.P. gratefully acknowledges NASA award 80NSSC22M0024.

This research has made use of the NASA Exoplanet Archive, which is operated by the California Institute of Technology, under contract with the National Aeronautics and Space Administration under the Exoplanet Exploration Program. This paper includes data collected by the Kepler mission and obtained from the MAST data archive at the Space Telescope Science Institute (STScI). Funding for the Kepler mission is provided by the NASA Science Mission Directorate. STScI is operated by the Association of Universities for Research in Astronomy, Inc., under NASA contract NAS 5–26555. This research has made use of the Exoplanet Follow-up Observation Program (ExoFOP; DOI: 10.26134/ExoFOP5) website, which is operated by the California Institute of Technology, under contract with the National Aeronautics and Space Administration under the Exoplanet Exploration Program.

Some of the data presented herein were obtained at the W. M. Keck Observatory, which is operated as a scientific partnership among the California Institute of Technology, the University of California, and NASA. The Observatory was made possible by the generous financial support of the W. M. Keck Foundation. Some of the Keck data were obtained under PI Data awards 2013A and 2013B (M. Payne).

Facilities: Keck:I (HIRES), Kepler

Software: `astropy` (Astropy Collaboration et al. 2013, 2018), `corner` (Foreman-Mackey 2016), `EXOFASTv2` (Eastman et al. 2013; Eastman 2017; Eastman et al. 2019), `lightkurve` (Lightkurve Collaboration et al. 2018), `RadVel` (Fulton et al. 2018) `SpecMatch` (Petigura 2015; Petigura et al. 2017), `pymc3` (Salvatier et al. 2016), `theano` (Theano Development Team 2016), `REBOUND` (Rein & Liu 2012), `SPOCK` (Tamayo et al. 2020), `exoplanet` (Agol et al. 2020; Kipping 2013; Foreman-Mackey et al. 2021b; Foreman-Mackey et al. 2021), `celerite2` (Foreman-Mackey et al. 2017; Foreman-Mackey 2018), `starry` (Luger et al. 2019), `arviz` (Kumar et al. 2019)

REFERENCES

- Agol, E., Luger, R., & Foreman-Mackey, D. 2020, AJ, 159, 123, doi: [10.3847/1538-3881/ab4fee](https://doi.org/10.3847/1538-3881/ab4fee)
- Akeson, R. L., Chen, X., Ciardi, D., et al. 2013, PASP, 125, 989, doi: [10.1086/672273](https://doi.org/10.1086/672273)
- Ali-Dib, M., Cumming, A., & Lin, D. N. C. 2020, MNRAS, 494, 2440, doi: [10.1093/mnras/staa914](https://doi.org/10.1093/mnras/staa914)
- Angus, R., Morton, T., Aigrain, S., Foreman-Mackey, D., & Rajpaul, V. 2018, MNRAS, 474, 2094, doi: [10.1093/mnras/stx2109](https://doi.org/10.1093/mnras/stx2109)
- Astropy Collaboration, Robitaille, T. P., Tollerud, E. J., et al. 2013, A&A, 558, A33, doi: [10.1051/0004-6361/201322068](https://doi.org/10.1051/0004-6361/201322068)

- Astropy Collaboration, Price-Whelan, A. M., Sipőcz, B. M., et al. 2018, *AJ*, 156, 123, doi: [10.3847/1538-3881/aabc4f](https://doi.org/10.3847/1538-3881/aabc4f)
- Bailey, A., & Zhu, Z. 2023, arXiv e-prints, arXiv:2310.03117, doi: [10.48550/arXiv.2310.03117](https://doi.org/10.48550/arXiv.2310.03117)
- Berger, T. A., Huber, D., van Saders, J. L., et al. 2020, *AJ*, 159, 280, doi: [10.3847/1538-3881/159/6/280](https://doi.org/10.3847/1538-3881/159/6/280)
- Berger, T. A., Schlieder, J. E., & Huber, D. 2023, arXiv e-prints, arXiv:2301.11338, doi: [10.48550/arXiv.2301.11338](https://doi.org/10.48550/arXiv.2301.11338)
- Bergez-Casalou, C., Bitsch, B., & Raymond, S. N. 2023, *A&A*, 669, A129, doi: [10.1051/0004-6361/202244988](https://doi.org/10.1051/0004-6361/202244988)
- Bitsch, B., Morbidelli, A., Johansen, A., et al. 2018, *A&A*, 612, A30, doi: [10.1051/0004-6361/201731931](https://doi.org/10.1051/0004-6361/201731931)
- Borucki, W. J., Koch, D., Basri, G., et al. 2010, *Science*, 327, 977, doi: [10.1126/science.1185402](https://doi.org/10.1126/science.1185402)
- Bryan, M. L., Knutson, H. A., Lee, E. J., et al. 2019, *AJ*, 157, 52, doi: [10.3847/1538-3881/aa57f](https://doi.org/10.3847/1538-3881/aa57f)
- Butler, R. P., Marcy, G. W., Williams, E., et al. 1996, *PASP*, 108, 500, doi: [10.1086/133755](https://doi.org/10.1086/133755)
- Butler, R. P., Vogt, S. S., Laughlin, G., et al. 2017, *AJ*, 153, 208, doi: [10.3847/1538-3881/aa66ca](https://doi.org/10.3847/1538-3881/aa66ca)
- Caldirolì, A., Haardt, F., Gallo, E., et al. 2022, *A&A*, 663, A122, doi: [10.1051/0004-6361/202142763](https://doi.org/10.1051/0004-6361/202142763)
- Carrera, D., Raymond, S. N., & Davies, M. B. 2019, *A&A*, 629, L7, doi: [10.1051/0004-6361/201935744](https://doi.org/10.1051/0004-6361/201935744)
- Chachan, Y., Lee, E. J., & Knutson, H. A. 2021, *ApJ*, 919, 63, doi: [10.3847/1538-4357/ac0bb6](https://doi.org/10.3847/1538-4357/ac0bb6)
- Chen, Y.-X., Li, Y.-P., Li, H., & Lin, D. N. C. 2020, *ApJ*, 896, 135, doi: [10.3847/1538-4357/ab9604](https://doi.org/10.3847/1538-4357/ab9604)
- Choi, J., Dotter, A., Conroy, C., et al. 2016, *ApJ*, 823, 102, doi: [10.3847/0004-637X/823/2/102](https://doi.org/10.3847/0004-637X/823/2/102)
- Cranmer, M., Tamayo, D., Rein, H., et al. 2021, *Proceedings of the National Academy of Science*, 118, e2026053118, doi: [10.1073/pnas.2026053118](https://doi.org/10.1073/pnas.2026053118)
- Dalba, P. A., Kane, S. R., Isaacson, H., et al. 2021a, *AJ*, 161, 103, doi: [10.3847/1538-3881/abd408](https://doi.org/10.3847/1538-3881/abd408)
- Dalba, P. A., Kane, S. R., Li, Z., et al. 2021b, *AJ*, 162, 154, doi: [10.3847/1538-3881/ac134b](https://doi.org/10.3847/1538-3881/ac134b)
- Dawson, R. I., Lee, E. J., & Chiang, E. 2016, *ApJ*, 822, 54, doi: [10.3847/0004-637X/822/1/54](https://doi.org/10.3847/0004-637X/822/1/54)
- Díaz, R. F., Ségransan, D., Udry, S., et al. 2016, *A&A*, 585, A134, doi: [10.1051/0004-6361/201526729](https://doi.org/10.1051/0004-6361/201526729)
- Dotter, A. 2016, *ApJS*, 222, 8, doi: [10.3847/0067-0049/222/1/8](https://doi.org/10.3847/0067-0049/222/1/8)
- Duffell, P. C., & MacFadyen, A. I. 2013, *ApJ*, 769, 41, doi: [10.1088/0004-637X/769/1/41](https://doi.org/10.1088/0004-637X/769/1/41)
- Eastman, J. 2017, EXOFASTv2: Generalized publication-quality exoplanet modeling code, v2, Astrophysics Source Code Library. <http://ascl.net/1710.003>
- Eastman, J., Gaudi, B. S., & Agol, E. 2013, *PASP*, 125, 83, doi: [10.1086/669497](https://doi.org/10.1086/669497)
- Eastman, J. D., Rodriguez, J. E., Agol, E., et al. 2019, arXiv e-prints. <https://arxiv.org/abs/1907.09480>
- Espinoza, N., Kossakowski, D., & Brahm, R. 2019, *MNRAS*, 490, 2262, doi: [10.1093/mnras/stz2688](https://doi.org/10.1093/mnras/stz2688)
- Fischer, D. A., & Valenti, J. 2005, *ApJ*, 622, 1102, doi: [10.1086/428383](https://doi.org/10.1086/428383)
- Foreman-Mackey, D. 2016, *The Journal of Open Source Software*, 24, doi: [10.21105/joss.00024](https://doi.org/10.21105/joss.00024)
- Foreman-Mackey, D. 2018, *Research Notes of the American Astronomical Society*, 2, 31, doi: [10.3847/2515-5172/aaaf6c](https://doi.org/10.3847/2515-5172/aaaf6c)
- Foreman-Mackey, D., Agol, E., Ambikasaran, S., & Angus, R. 2017, *AJ*, 154, 220, doi: [10.3847/1538-3881/aa9332](https://doi.org/10.3847/1538-3881/aa9332)
- Foreman-Mackey, D., Luger, R., Agol, E., et al. 2021a, arXiv e-prints, arXiv:2105.01994. <https://arxiv.org/abs/2105.01994>
- . 2021b, arXiv e-prints, arXiv:2105.01994. <https://arxiv.org/abs/2105.01994>
- Foreman-Mackey, D., Savel, A., Luger, R., et al. 2021, *exoplanet-dev/exoplanet v0.5.1*, doi: [10.5281/zenodo.1998447](https://doi.org/10.5281/zenodo.1998447)
- Fulton, B. J., Petigura, E. A., Blunt, S., & Sinukoff, E. 2018, *PASP*, 130, 044504, doi: [10.1088/1538-3873/aaaaa8](https://doi.org/10.1088/1538-3873/aaaaa8)
- Fulton, B. J., Collins, K. A., Gaudi, B. S., et al. 2015, *ApJ*, 810, 30, doi: [10.1088/0004-637X/810/1/30](https://doi.org/10.1088/0004-637X/810/1/30)
- Fung, J., Shi, J.-M., & Chiang, E. 2014, *ApJ*, 782, 88, doi: [10.1088/0004-637X/782/2/88](https://doi.org/10.1088/0004-637X/782/2/88)
- Furlan, E., Ciardi, D. R., Everett, M. E., et al. 2017, *AJ*, 153, 71, doi: [10.3847/1538-3881/153/2/71](https://doi.org/10.3847/1538-3881/153/2/71)
- Gaia Collaboration, Prusti, T., de Bruijne, J. H. J., et al. 2016, *A&A*, 595, A1, doi: [10.1051/0004-6361/201629272](https://doi.org/10.1051/0004-6361/201629272)
- Gaia Collaboration, Brown, A. G. A., Vallenari, A., et al. 2018, *A&A*, 616, A1, doi: [10.1051/0004-6361/201833051](https://doi.org/10.1051/0004-6361/201833051)
- Gaia Collaboration, Vallenari, A., Brown, A. G. A., et al. 2022, arXiv e-prints, arXiv:2208.00211, doi: [10.48550/arXiv.2208.00211](https://doi.org/10.48550/arXiv.2208.00211)
- Goldreich, P., & Tremaine, S. 1980, *ApJ*, 241, 425, doi: [10.1086/158356](https://doi.org/10.1086/158356)
- Griveaud, P., Crida, A., & Lega, E. 2023, arXiv e-prints, arXiv:2303.04652. <https://arxiv.org/abs/2303.04652>
- Guillot, T., Santos, N. C., Pont, F., et al. 2006, *A&A*, 453, L21, doi: [10.1051/0004-6361:20065476](https://doi.org/10.1051/0004-6361:20065476)
- Gundlach, B., Schmidt, K. P., Kreuzig, C., et al. 2018, *MNRAS*, 479, 1273, doi: [10.1093/mnras/sty1550](https://doi.org/10.1093/mnras/sty1550)
- Hadden, S., & Lithwick, Y. 2018, *AJ*, 156, 95, doi: [10.3847/1538-3881/aad32c](https://doi.org/10.3847/1538-3881/aad32c)
- Hasegawa, Y., Bryden, G., Ikoma, M., Vasisht, G., & Swain, M. 2018, *ApJ*, 865, 32, doi: [10.3847/1538-4357/aad912](https://doi.org/10.3847/1538-4357/aad912)

- Holczer, T., Mazeh, T., Nachmani, G., et al. 2016, *ApJS*, 225, 9, doi: [10.3847/0067-0049/225/1/9](https://doi.org/10.3847/0067-0049/225/1/9)
- Howard, A. W., Johnson, J. A., Marcy, G. W., et al. 2010, *ApJ*, 721, 1467, doi: [10.1088/0004-637X/721/2/1467](https://doi.org/10.1088/0004-637X/721/2/1467)
- Ikoma, M., Emori, H., & Nakazawa, K. 2001, *ApJ*, 553, 999, doi: [10.1086/320954](https://doi.org/10.1086/320954)
- Isaacson, H., & Fischer, D. 2010, *ApJ*, 725, 875, doi: [10.1088/0004-637X/725/1/875](https://doi.org/10.1088/0004-637X/725/1/875)
- Jenkins, J. M., Caldwell, D. A., Chandrasekaran, H., et al. 2010, *ApJL*, 713, L87, doi: [10.1088/2041-8205/713/2/L87](https://doi.org/10.1088/2041-8205/713/2/L87)
- Johnstone, C. P., Bartel, M., & Güdel, M. 2021, *A&A*, 649, A96, doi: [10.1051/0004-6361/202038407](https://doi.org/10.1051/0004-6361/202038407)
- Kimura, H., Wada, K., Yoshida, F., et al. 2020, *MNRAS*, 1682, 1667, doi: [10.1093/mnras/staa1641](https://doi.org/10.1093/mnras/staa1641)
- Kipping, D. M. 2013, *MNRAS*, 435, 2152, doi: [10.1093/mnras/stt1435](https://doi.org/10.1093/mnras/stt1435)
- Kolbl, R., Marcy, G. W., Isaacson, H., & Howard, A. W. 2015, *AJ*, 149, 18, doi: [10.1088/0004-6256/149/1/18](https://doi.org/10.1088/0004-6256/149/1/18)
- Kraus, A. L., Ireland, M. J., Huber, D., Mann, A. W., & Dupuy, T. J. 2016, *AJ*, 152, 8, doi: [10.3847/0004-6256/152/1/8](https://doi.org/10.3847/0004-6256/152/1/8)
- Kumar, R., Carroll, C., Hartikainen, A., & Martin, O. A. 2019, *The Journal of Open Source Software*, doi: [10.21105/joss.01143](https://doi.org/10.21105/joss.01143)
- Lammers, C., Hadden, S., & Murray, N. 2024, arXiv e-prints, arXiv:2403.17928, doi: [10.48550/arXiv.2403.17928](https://doi.org/10.48550/arXiv.2403.17928)
- Lee, E. J., & Chiang, E. 2015, *ApJ*, 811, 41, doi: [10.1088/0004-637X/811/1/41](https://doi.org/10.1088/0004-637X/811/1/41)
- . 2016, *ApJ*, 817, 90, doi: [10.3847/0004-637X/817/2/90](https://doi.org/10.3847/0004-637X/817/2/90)
- Lee, E. J., & Connors, N. J. 2021, *ApJ*, 908, 32, doi: [10.3847/1538-4357/abd6c7](https://doi.org/10.3847/1538-4357/abd6c7)
- Lee, J.-M., Irwin, P. G. J., Fletcher, L. N., Heng, K., & Barstow, J. K. 2014, *ApJ*, 789, 14, doi: [10.1088/0004-637X/789/1/14](https://doi.org/10.1088/0004-637X/789/1/14)
- Lightkurve Collaboration, Cardoso, J. V. d. M., Hedges, C., et al. 2018, *Lightkurve: Kepler and TESS time series analysis in Python, 1.11*, *Astrophysics Source Code Library*. <http://ascl.net/1812.013>
- Lithwick, Y., & Naoz, S. 2011, *ApJ*, 742, 94, doi: [10.1088/0004-637X/742/2/94](https://doi.org/10.1088/0004-637X/742/2/94)
- Lopez, E. D., Fortney, J. J., & Miller, N. 2012, *ApJ*, 761, 59, doi: [10.1088/0004-637X/761/1/59](https://doi.org/10.1088/0004-637X/761/1/59)
- Lovis, C., Dumusque, X., Santos, N. C., et al. 2011, arXiv e-prints, arXiv:1107.5325, doi: [10.48550/arXiv.1107.5325](https://doi.org/10.48550/arXiv.1107.5325)
- Luger, R., Agol, E., Foreman-Mackey, D., et al. 2019, *AJ*, 157, 64, doi: [10.3847/1538-3881/aae8e5](https://doi.org/10.3847/1538-3881/aae8e5)
- Mann, C. R., Dalba, P. A., Lafrenière, D., et al. 2023, *AJ*, 166, 239, doi: [10.3847/1538-3881/ad00bc](https://doi.org/10.3847/1538-3881/ad00bc)
- Miguel, Y., Guilera, O. M., & Brunini, A. 2011, *MNRAS*, 417, 314, doi: [10.1111/j.1365-2966.2011.19264.x](https://doi.org/10.1111/j.1365-2966.2011.19264.x)
- Moldenhauer, T. W., Kuiper, R., Kley, W., & Ormel, C. W. 2021, *A&A*, 646, L11, doi: [10.1051/0004-6361/202040220](https://doi.org/10.1051/0004-6361/202040220)
- Morton, T. D., Bryson, S. T., Coughlin, J. L., et al. 2016, *ApJ*, 822, 86, doi: [10.3847/0004-637X/822/2/86](https://doi.org/10.3847/0004-637X/822/2/86)
- Mousis, O., Marboeuf, U., Lunine, J. I., et al. 2009, *ApJ*, 696, 1348, doi: [10.1088/0004-637X/696/2/1348](https://doi.org/10.1088/0004-637X/696/2/1348)
- Musiolik, G., & Wurm, G. 2019, *ApJ*, 873, 58, doi: [10.3847/1538-4357/ab0428](https://doi.org/10.3847/1538-4357/ab0428)
- Öberg, K. I., Murray-Clay, R., & Bergin, E. A. 2011, *ApJL*, 743, L16, doi: [10.1088/2041-8205/743/1/L16](https://doi.org/10.1088/2041-8205/743/1/L16)
- Ormel, C. W. 2014, *ApJL*, 789, L18, doi: [10.1088/2041-8205/789/1/L18](https://doi.org/10.1088/2041-8205/789/1/L18)
- Ormel, C. W., Shi, J.-M., & Kuiper, R. 2015, *MNRAS*, 447, 3512, doi: [10.1093/mnras/stu2704](https://doi.org/10.1093/mnras/stu2704)
- Paxton, B., Bildsten, L., Dotter, A., et al. 2011, *ApJS*, 192, 3, doi: [10.1088/0067-0049/192/1/3](https://doi.org/10.1088/0067-0049/192/1/3)
- Paxton, B., Cantiello, M., Arras, P., et al. 2013, *ApJS*, 208, 4, doi: [10.1088/0067-0049/208/1/4](https://doi.org/10.1088/0067-0049/208/1/4)
- Paxton, B., Marchant, P., Schwab, J., et al. 2015, *ApJS*, 220, 15, doi: [10.1088/0067-0049/220/1/15](https://doi.org/10.1088/0067-0049/220/1/15)
- Petigura, E. A. 2015, PhD thesis, University of California, Berkeley
- Petigura, E. A., Howard, A. W., Marcy, G. W., et al. 2017, *AJ*, 154, 107, doi: [10.3847/1538-3881/aa80de](https://doi.org/10.3847/1538-3881/aa80de)
- Petit, A. C., Pichierri, G., Davies, M. B., & Johansen, A. 2020, *A&A*, 641, A176, doi: [10.1051/0004-6361/202038764](https://doi.org/10.1051/0004-6361/202038764)
- Piso, A.-M. A., Youdin, A. N., & Murray-Clay, R. A. 2015, *ApJ*, 800, 82, doi: [10.1088/0004-637X/800/2/82](https://doi.org/10.1088/0004-637X/800/2/82)
- Pollack, J. B., Hubickyj, O., Bodenheimer, P., et al. 1996, *Icarus*, 124, 62, doi: [10.1006/icar.1996.0190](https://doi.org/10.1006/icar.1996.0190)
- Pu, B., & Lai, D. 2018, *MNRAS*, 478, 197, doi: [10.1093/mnras/sty1098](https://doi.org/10.1093/mnras/sty1098)
- Pu, B., & Wu, Y. 2015, *ApJ*, 807, 44, doi: [10.1088/0004-637X/807/1/44](https://doi.org/10.1088/0004-637X/807/1/44)
- Rafikov, R. R. 2006, *ApJ*, 648, 666, doi: [10.1086/505695](https://doi.org/10.1086/505695)
- Rasio, F. A., & Ford, E. B. 1996, *Science*, 274, 954, doi: [10.1126/science.274.5289.954](https://doi.org/10.1126/science.274.5289.954)
- Rein, H., & Liu, S. F. 2012, *A&A*, 537, A128, doi: [10.1051/0004-6361/201118085](https://doi.org/10.1051/0004-6361/201118085)
- Rosenthal, L. J., Fulton, B. J., Hirsch, L. A., et al. 2021, *ApJS*, 255, 8, doi: [10.3847/1538-4365/abe23c](https://doi.org/10.3847/1538-4365/abe23c)
- Salvatier, J., Wiecki, T. V., & Fonnesbeck, C. 2016, *PeerJ Computer Science*, 2, e55
- Savignac, V., & Lee, E. J. 2023, arXiv e-prints, arXiv:2310.06013, doi: [10.48550/arXiv.2310.06013](https://doi.org/10.48550/arXiv.2310.06013)
- Schlafly, E. F., & Finkbeiner, D. P. 2011, *ApJ*, 737, 103, doi: [10.1088/0004-637X/737/2/103](https://doi.org/10.1088/0004-637X/737/2/103)

- Smith, J. C., Stumpe, M. C., Van Cleve, J. E., et al. 2012, *PASP*, 124, 1000, doi: [10.1086/667697](https://doi.org/10.1086/667697)
- Sobski, N., & Millholland, S. C. 2023, *ApJ*, 954, 137, doi: [10.3847/1538-4357/ace966](https://doi.org/10.3847/1538-4357/ace966)
- Stevenson, D. J. 1982, *Planet. Space Sci.*, 30, 755. https://ac.els-cdn.com/0032063382901088/1-s2.0-0032063382901088-main.pdf?{}_tid=12d3dd2d-35b5-4b63-b3fc-541121433ade{&}acdnat=1524542327{_-}d09183c81d97256b4f80b209b8774a04
- Stumpe, M. C., Smith, J. C., Van Cleve, J. E., et al. 2012, *PASP*, 124, 985, doi: [10.1086/667698](https://doi.org/10.1086/667698)
- Tamayo, D., Cranmer, M., Hadden, S., et al. 2020, *Proceedings of the National Academy of Science*, 117, 18194, doi: [10.1073/pnas.2001258117](https://doi.org/10.1073/pnas.2001258117)
- Tayar, J., Claytor, Z. R., Huber, D., & van Saders, J. 2020, arXiv e-prints, arXiv:2012.07957. <https://arxiv.org/abs/2012.07957>
- Theano Development Team. 2016, arXiv e-prints, abs/1605.02688. <http://arxiv.org/abs/1605.02688>
- Thompson, S. E., Coughlin, J. L., Hoffman, K., et al. 2018, *ApJS*, 235, 38, doi: [10.3847/1538-4365/aab4f9](https://doi.org/10.3847/1538-4365/aab4f9)
- Thorngren, D., & Fortney, J. J. 2019, *ApJL*, 874, L31, doi: [10.3847/2041-8213/ab1137](https://doi.org/10.3847/2041-8213/ab1137)
- Thorngren, D. P., Fortney, J. J., Murray-Clay, R. A., & Lopez, E. D. 2016, *ApJ*, 831, 64, doi: [10.3847/0004-637X/831/1/64](https://doi.org/10.3847/0004-637X/831/1/64)
- Thorngren, D. P., Lee, E. J., & Lopez, E. D. 2023, *ApJL*, 945, L36, doi: [10.3847/2041-8213/acbd35](https://doi.org/10.3847/2041-8213/acbd35)
- Torres, G., Fischer, D. A., Sozzetti, A., et al. 2012, *ApJ*, 757, 161, doi: [10.1088/0004-637X/757/2/161](https://doi.org/10.1088/0004-637X/757/2/161)
- Tsiganis, K., Gomes, R., Morbidelli, A., & Levison, H. F. 2005, *Nature*, 435, 459, doi: [10.1038/nature03539](https://doi.org/10.1038/nature03539)
- Valizadegan, H., Martinho, M. J. S., Wilkens, L. S., et al. 2022, *ApJ*, 926, 120, doi: [10.3847/1538-4357/ac4399](https://doi.org/10.3847/1538-4357/ac4399)
- Vogt, S. S., Allen, S. L., Bigelow, B. C., et al. 1994, in *Proc. SPIE*, Vol. 2198, Instrumentation in Astronomy VIII, ed. D. L. Crawford & E. R. Craine, 362, doi: [10.1117/12.176725](https://doi.org/10.1117/12.176725)
- Walsh, K. J., Morbidelli, A., Raymond, S. N., O'Brien, D. P., & Mandell, A. M. 2011, *Nature*, 475, 206, doi: [10.1038/nature10201](https://doi.org/10.1038/nature10201)
- Winn, J. N., Albrecht, S., Johnson, J. A., et al. 2011, *ApJL*, 741, L1, doi: [10.1088/2041-8205/741/1/L1](https://doi.org/10.1088/2041-8205/741/1/L1)
- Wisdom, J. 1980, *AJ*, 85, 1122, doi: [10.1086/112778](https://doi.org/10.1086/112778)
- Wright, J. T., Marcy, G. W., Butler, R. P., & Vogt, S. S. 2004, *ApJS*, 152, 261, doi: [10.1086/386283](https://doi.org/10.1086/386283)
- Wu, Y., & Murray, N. 2003, *ApJ*, 589, 605, doi: [10.1086/374598](https://doi.org/10.1086/374598)
- Zhu, W. 2022, *AJ*, 164, 5, doi: [10.3847/1538-3881/ac6f59](https://doi.org/10.3847/1538-3881/ac6f59)
- Zhu, W., & Wu, Y. 2018, *AJ*, 156, 92, doi: [10.3847/1538-3881/aad22a](https://doi.org/10.3847/1538-3881/aad22a)
- Zhu, Z., Jiang, Y.-F., Baehr, H., et al. 2021, *MNRAS*, 508, 453, doi: [10.1093/mnras/stab2517](https://doi.org/10.1093/mnras/stab2517)